

## Spin Hall Effect and Origins of Nonlocal Resistance in Adatom-Decorated Graphene

D. Van Tuan,<sup>1,2</sup> J. M. Marmolejo-Tejada,<sup>3,4</sup> X. Waintal,<sup>5</sup> B. K. Nikolić,<sup>3,\*</sup> S. O. Valenzuela,<sup>1,6</sup> and S. Roche<sup>1,6,†</sup>

<sup>1</sup>*Catalan Institute of Nanoscience and Nanotechnology (ICN2), CSIC and The Barcelona Institute of Science and Technology, Campus UAB, Bellaterra, 08193 Barcelona, Spain*

<sup>2</sup>*Department of Electrical and Computer Engineering, University of Rochester, Rochester, New York 14627, USA*

<sup>3</sup>*Department of Physics and Astronomy, University of Delaware, Newark, Delaware 19716-2570, USA*

<sup>4</sup>*School of Electrical and Electronics Engineering, Universidad del Valle, Cali AA 25360, Colombia*

<sup>5</sup>*Univ. Grenoble Alpes, INAC-PHELIQS, F-38000 Grenoble, France and CEA, INAC-PHELIQS, F-38000 Grenoble, France*

<sup>6</sup>*ICREA—Institució Catalana de Recerca i Estudis Avançats, 08010 Barcelona, Spain*

(Received 19 February 2016; published 20 October 2016)

Recent experiments reporting an unexpectedly large spin Hall effect (SHE) in graphene decorated with adatoms have raised a fierce controversy. We apply numerically exact Kubo and Landauer-Büttiker formulas to realistic models of gold-decorated disordered graphene (including adatom clustering) to obtain the spin Hall conductivity and spin Hall angle, as well as the nonlocal resistance as a quantity accessible to experiments. Large spin Hall angles of  $\sim 0.1$  are obtained at zero temperature, but their dependence on adatom clustering differs from the predictions of semiclassical transport theories. Furthermore, we find multiple background contributions to the nonlocal resistance, some of which are unrelated to the SHE or any other spin-dependent origin, as well as a strong suppression of the SHE at room temperature. This motivates us to design a multiterminal graphene geometry which suppresses these background contributions and could, therefore, quantify the upper limit for spin-current generation in two-dimensional materials.

DOI: 10.1103/PhysRevLett.117.176602

Over the past decade, the spin Hall effect (SHE) has evolved rapidly from an obscure theoretical prediction to a major resource for spintronics [1,2]. In the direct SHE, the injection of a conventional unpolarized charge current into a material with extrinsic (due to impurities) or intrinsic (due to band structure) spin-orbit coupling (SOC) generates a pure spin current in the direction transverse to the charge current. Although the SHE was first observed only a decade ago [3], it is already ubiquitous within spintronics as the standard pure spin-current generator and detector [1,2]. The spin Hall angle  $\theta_{\text{SH}}$ , as the ratio of generated spin Hall current and injected charge current, is the figure of merit for charge-to-spin conversion efficiency. To date, measured values of  $\theta_{\text{SH}}$  range from  $\sim 10^{-4}$  in semiconductors to  $\sim 0.1$  in metals like  $\beta$ -Ta and  $\beta$ -W [2].

Concurrently, the discovery of graphene [4] has ignited a considerable amount of activity, owing to its unique electronic properties and versatility for practical applications, including possible applications in spintronics [5]. The intrinsically small SOC and hyperfine interactions [6] in graphene lead to spin relaxation lengths reaching several tens of micrometers at room temperature [7–10] but simultaneously making pristine graphene inactive for the SHE [5]. On the other hand, recent nonlocal transport measurements on graphene decorated with heavy adatoms like copper, gold, and silver have extracted exceptionally large values for  $\theta_{\text{SH}} \sim 0.2$  [11]. These reports follow prior experiments on weakly hydrogenated graphene, which showed surprisingly similar results [12] despite using light

adatoms like hydrogen. The large values of  $\theta_{\text{SH}}$  observed in both types of experiments have been supported by semiclassical transport theories [13,14].

The very recent experiments [15,16] aiming to reproduce these results have indeed confirmed a large nonlocal transport signal near the charge neutral point (CNP) of graphene which, however, appears to be disconnected from SHE physics or any other spin-related mechanism. For example, Wang and co-workers [15] reported that Au- or Ir-decorated graphene exhibits no signature of the SHE and relate the large nonlocal resistance  $R_{\text{NL}}$  to the formation of neutral Hall currents. Kaverzin and van Wees [16] found large  $R_{\text{NL}}$  in hydrogenated graphene which was insensitive to an applied in-plane magnetic field. These authors [16] exclude the valley Hall effect and long-range chargeless valley currents [17] as mediating such  $R_{\text{NL}}$ , given the absence of both its temperature dependence and broken inversion symmetry, and conclude that a nontrivial and unknown phenomenon is at play.

The presently available theories for  $\theta_{\text{SH}}$  [13] or  $R_{\text{NL}}$  [18] offer little guidance on how to resolve these controversies, since they utilize semiclassical approaches to charge transport and spin relaxation which are known to break down [19,20] near the CNP. Moreover, while the Kubo formula [21] offers a fully quantum-mechanical treatment that can, in principle, capture all relevant effects, its standard analytic evaluation [22] neglects terms (such as those corresponding to skew scattering from pairs of closely spaced impurities [23]) in the perturbative expansion in

disorder strength which can become crucial for clusters of adatoms. Finally, the impact of unavoidable adatom clustering [24] on  $\theta_{\text{SH}}$  is an open and important question, since adatom segregation has been shown to strongly affect spin transport properties [25,26].

In this Letter, the spin Hall angle in graphene decorated with Au adatoms is computed by using two different *numerically exact* quantum transport methodologies—the real-space Kubo formula and the multiterminal Landauer-Büttiker (LB) formula [27]. At zero temperature, both methods yield  $\theta_{\text{SH}} \sim 0.1\text{--}0.3$  for the same Au-adatom concentration  $n_i$ . However, those values require rather large  $n_i \gtrsim 10\%$  and drop significantly when temperature and adatom clustering are taken into account.

Furthermore, the LB formula applied to six-terminal graphene geometry in Fig. 1 reveals large background contributions to  $R_{\text{NL}}$  even when *SOC is artificially turned off*. They are, therefore, unrelated to SHE physics and are also unrelated to the trivial Ohmic contribution due to classical current paths [16,18]. We show that their sign [28,29] and scaling with the channel length  $L$  make it possible to understand their origin. This allows us to propose a novel six-terminal graphene setup—see Fig. S7 in Supplemental Material [30]—where such background contributions can be eliminated in order to study a purely SHE-driven  $R_{\text{NL}}$  signal.

*Hamiltonian model for Au-decorated graphene.*—When an adatom like gold, thallium or indium is absorbed onto a graphene surface, it resides in the center of graphene carbon rings where it can enhance the intrinsic SOC or induce Rashba SOC due to the broken inversion symmetry [34]. The minimal (with a single  $\pi$  orbital per site) effective tight-binding model for graphene with such adatoms is given by

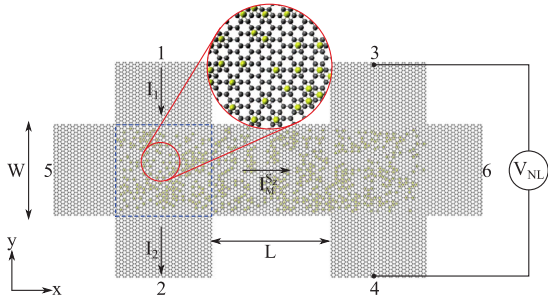


FIG. 1. Schematic view of a six-terminal graphene employed to compute the nonlocal resistance  $R_{\text{NL}} = V_{\text{NL}}/I_1$  and the spin Hall angle  $\theta_{\text{SH}} = I_5^S/I_1$ . For nonlocal transport, the injected transverse charge current between leads 1 and 2 generates the longitudinal spin current  $I_5^S$  in lead 5 as well as the mediative spin current  $I_M^S$ , whose conversion into the voltage drop  $V_{\text{NL}} = V_3 - V_4$  between leads 3 and 4 generates  $R_{\text{NL}}$ . The dashed region illustrates the sample of size  $400 \text{ nm} \times 400 \text{ nm}$ , with periodic boundary conditions, used for calculations of Kubo conductivities. The enlargement shows carbon atoms (black circles) and Au adatoms (yellow circles).

$$\mathcal{H} = -\gamma_0 \sum_{\langle ij \rangle} c_i^\dagger c_j + \frac{2i}{\sqrt{3}} V_I \sum_{\langle\langle ij \rangle\rangle \in \mathcal{R}} c_i^\dagger \vec{s} \cdot (\vec{d}_{kj} \times \vec{d}_{ik}) c_j + iV_R \sum_{\langle ij \rangle \in \mathcal{R}} c_i^\dagger \vec{z} \cdot (\vec{s} \times \vec{d}_{ij}) c_j - \mu \sum_{i \in \mathcal{R}} c_i^\dagger c_i. \quad (1)$$

The first term is the nearest-neighbor hopping term with  $\gamma_0 = 2.7 \text{ eV}$ . The second term is the next-nearest-neighbor hopping term, which accounts for the local intrinsic SOC enhancement by adatoms residing on the set of hexagons  $\mathcal{R}$ . The unit vector  $\vec{d}_{kj}$  points from atom  $j$  to atom  $k$ , with atom  $k$  standing in between  $i$  and  $j$ , and  $\vec{s} = (s_x, s_y, s_z)$  is the vector of the Pauli matrices. The third term is the nearest-neighbor hopping term describing the Rashba SOC which explicitly violates  $\vec{z} \rightarrow -\vec{z}$  symmetry. The last term is the on-site potential  $\mu$  on carbon atoms in the hexagons hosting adatoms, which simulates charge modulation induced locally around the adatom [34]. The Hamiltonian in Eq. (1) has been employed to study spin dynamics in graphene decorated with Au adatoms [19], and here we use the same parameters  $V_I = 0.007\gamma_0$ ,  $V_R = 0.0165\gamma_0$ , and  $\mu = 0.1\gamma_0$  fitted to first-principles calculations [34].

Figure 1 shows the geometry used for the calculations of bulk Kubo conductivities and multiterminal charge and spin currents. The calculations of  $\theta_{\text{SH}}$  with the Kubo formula are performed using a graphene flake of the size  $400 \text{ nm} \times 400 \text{ nm}$  enclosed in a dashed square with periodic boundary conditions. For LB calculations, we consider full six-terminal geometry in Fig. 1, where the central region with edges of armchair type, width  $W = 50 \text{ nm}$  (composed of  $3n + 2$  dimer lines, so that its electronic structure resembles that of large-area graphene [20]), and variable distance  $L$  between the pair of leads 1 and 2 and the pair of leads 3 and 4 is attached to two armchair longitudinal leads and four transverse leads with zigzag edges and of width  $W = 50 \text{ nm}$ . Akin to the experimental procedure [11,12,15,16,35], injecting unpolarized charge current  $I_1$  into this measurement geometry induces  $R_{\text{NL}} = (V_3 - V_4)/I_1$  and  $\theta_{\text{SH}} = I_5^S/I_1$ .

*Real-space Kubo formula for spin Hall conductivity.*—The Kubo formula for spin Hall conductivity  $\sigma_{\text{SH}}$  reads [2]

$$\sigma_{\text{SH}} = \frac{e\hbar}{\Omega} \sum_{m,n} \frac{f(E_m) - f(E_n)}{E_m - E_n} \frac{\text{Im}[\langle m | J_x^z | n \rangle \langle n | v_y | m \rangle]}{E_m - E_n + i\eta}, \quad (2)$$

where  $v_x$  is the velocity operator and  $J_x^z = (\hbar/4)\{s_z, v_x\}$  is the spin-current operator. The numerical evaluation of Eq. (2) is usually made by finding the whole spectrum  $E_m$  and the full set of eigenvectors  $\{|m\rangle\}$  of  $\mathcal{H}$ , which is a computationally expensive task. Here we develop an alternative and efficient real-space formalism by rewriting  $\sigma_{\text{SH}}$  as

$$\sigma_{\text{SH}} = \frac{e\hbar}{\Omega} \int dx dy \frac{f(x) - f(y)}{(x-y)^2 + \eta^2} j(x, y), \quad (3)$$

with  $j(x,y) = \sum_{m,n} \text{Im}[\langle m | J_x^z | n \rangle \langle n | v_y | m \rangle] \delta(x - E_m) \delta(y - E_n)$ . This can be calculated by rescaling  $\mathcal{H}$ ,  $x$ ,  $y$ , and  $E$  into the interval  $[-1, 1]$  (the corresponding variables are  $h$ ,  $\hat{x}$ ,  $\hat{y}$ , and  $\epsilon$ , respectively) and by expanding  $j(x, y)$  into Chebyshev polynomials  $T_m(\hat{x})$  as  $j(x, y) = \sum_{m,n}^M [4\mu_{mn} g_m g_n T_m(\hat{x}) \times T_n(\hat{y})] / [(1 + \delta_{m,0})(1 + \delta_{n,0}) \pi^2 \sqrt{(1 - \hat{x}^2)(1 - \hat{y}^2)}]$ , where  $\mu_{mn} = \text{Im}\{\text{Tr}[J_x^z T_n(h) v_y T_m(h)]\} / \Delta E^2$  and  $\Delta E$  is half the bandwidth [36]. Here  $g_m$  is the filter, Jackson kernel, that minimizes the Gibbs oscillations arising in truncating the series to finite order  $M$  [36]. The trace in  $\mu_{mn}$  is computed by averaging [37] over a small number  $r \ll N$  of random phase vectors  $|\varphi\rangle$ , with  $N$  being the number of carbon atoms considered in the sample. Hereafter,  $M = 1500$  ( $= 6000$ ) for  $\sigma_{\text{SH}}$  ( $\sigma_{xx}$ ),  $r = 1$ , and  $N = 4 \times 10^6$ . Similar methods have been developed for the longitudinal conductivity  $\sigma_{xx}$  [37], Hall conductivity  $\sigma_{xy}$  [38,39], and spin Hall conductivity  $\sigma_{\text{SH}}$  [40]. The method is validated by comparing our numerically evaluated  $\sigma_{\text{SH}}$  with analytic results [41] for clean graphene with homogeneous Rashba or intrinsic SOC [30].

*Spin Hall angle for different adatom distributions.*— Figure 2 shows  $\sigma_{\text{SH}}$  for  $n_i = 15\%$  of Au adatoms distributed in a scattered [Fig. 2(a)] or clustered fashion [Fig. 2(b)], where clusters are randomly distributed islands of radius  $\in [1, 3]$  nm. Although the random distribution of Au adatoms and the Rashba SOC associated with them induce scattering [ $\mu = 0.1\gamma_0$  in Eq. (1)], the dependence of  $\sigma_{\text{SH}}$  on the Fermi energy  $E_F$  in the absence of intrinsic SOC is reminiscent of a step behavior obtained for a homogeneous Rashba SOC [30], with  $\sigma_{\text{SH}} \approx \pm e/4\pi$  near the CNP. Adding a small intrinsic SOC,  $V_I = 0.007\gamma_0 \ll V_R$ , slightly changes the absolute value of  $\sigma_{\text{SH}}$  but preserves the step behavior. In contrast, the clustered distribution of

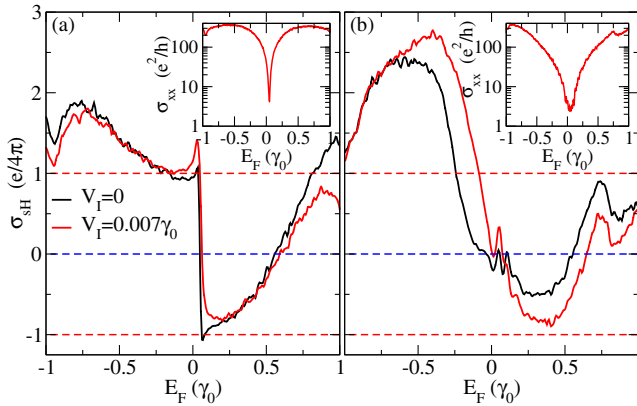


FIG. 2. Spin Hall  $\sigma_{\text{SH}}$  (main frame) and longitudinal  $\sigma_{xx}$  (insets) conductivities for the two cases of  $n_i = 15\%$  Au-adatom distributions: (a) scattered and (b) clustered, where Au islands have varying radius  $\in [1, 3]$  nm. In both cases, the effect of the presence (red lines,  $V_I = 0.007\gamma_0$ ) or absence (black lines,  $V_I = 0$ ) of the enhanced intrinsic SOC within the hexagons hosting adatoms is also shown. All results are averaged over 400 disorder configurations.

Au adatoms suppresses the step behavior and smooths out the shape of  $\sigma_{\text{SH}}$  close to the CNP. The effect of intrinsic SOC is more pronounced for the clustered distribution with a more significant enhancement of  $\sigma_{\text{SH}}$  on both the electron and the hole side.

The spin Hall angle  $\theta_{\text{SH}} = \sigma_{\text{SH}}/\sigma_{xx}$  requires the additional calculation of the longitudinal conductivity  $\sigma_{xx}$ , which is performed using a real-space Kubo formula [30]. Figure 2 (insets) shows  $\sigma_{xx}$  for both cases. Comparable values of  $\sigma_{xx}$  are obtained at the CNP, but for the scattered case  $\sigma_{xx}$  increases with energy faster than for the clustered case. Figure 3 shows  $\theta_{\text{SH}}$  for  $n_i = 15\%$  of Au adatoms, which are distributed homogeneously (black lines) or in clusters (red line). Remarkably, the values of  $\theta_{\text{SH}}$  shown in Fig. 3 are very large  $\sim 0.1$ – $0.3$  close to the CNP, which is similar to experimentally reported values [11]. At the CNP, a threefold decrease in  $\theta_{\text{SH}}$  is obtained when adatoms are clustered into islands with a small radius. This conclusion seems to differ from the semiclassical transport predictions, where  $\theta_{\text{SH}}$  increases with the radius of adatom clusters [13], although a strict comparison would require to treat a system consisting of identical islands. At higher energies, we observe a sizable  $\theta_{\text{SH}}$  for clustered adatoms, which contrasts with vanishingly small values for the scattered geometry. We finally extrapolate that, for  $n_i = 2\%$ – $3\%$  (as estimated in experiments [11]),  $\theta_{\text{SH}}$  should range between 0.01 and 0.1 (see Supplemental Material [30]). We stress, however, that our calculations represent an upper limit for experimental situations. There, the increase of the cluster size and the finite temperature can significantly decrease  $\theta_{\text{SH}}$  below 0.01 [30].

It is also instructive to compare the results in Fig. 2 to the case of heavier adatoms like thallium (Tl), which locally and substantially enhance the intrinsic SOC while generating negligible Rashba SOC [34]. A crossover from the quantum SHE to the conventional SHE has been predicted [26] when the distribution of Tl adatoms is changed from scattered to clustered. Figure S2 in Supplemental Material [30] shows that the SHE due to clustered Tl adatoms is

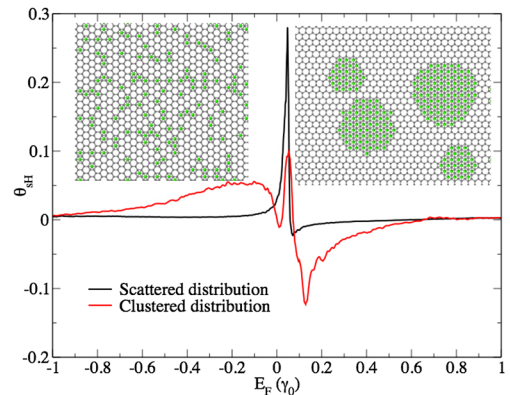


FIG. 3. Spin Hall angle  $\theta_{\text{SH}} = \sigma_{\text{SH}}/\sigma_{xx}$  corresponding to Fig. 2 for scattered (black curve) and clustered (red curve) distributions of Au adatoms, which are illustrated in the insets.

characterized by larger  $\theta_{\text{SH}}$  than in the case of either scattered or clustered Au adatoms.

*Nonlocal resistance and spin Hall angle in multiterminal graphene.*—In the SHE experiments [11,12], multiterminal graphene devices are employed to measure  $R_{\text{NL}}$ , as illustrated in Fig. 1. In such a circuit, a charge current  $I_1$  injected from lead 1 towards lead 2 generates the nonlocal resistance  $R_{\text{NL}} = (V_3 - V_4)/I_1$  at the Fermi energy  $E_F$  sufficiently close to the CNP. The appearance of nonzero  $R_{\text{NL}}$ , due to a SHE-driven mechanism, is explained by charge current  $I_1$  inducing mediative spin current  $I_M^{S_z}$  in the first crossbar in Fig. 1 flowing in the direction  $5 \rightarrow 6$ , which is subsequently converted into the nonlocal voltage  $V_{\text{NL}} = V_3 - V_4$  by the inverse SHE in the second crossbar. We calculate the total charge  $I_p$  and spin  $I_p^{S_z}$  currents and voltages  $V_p$  in leads  $p = 2-6$  in response to injected charge current  $I_1$  using the multiterminal LB formula [27], as implemented in the KWANT software package [30,42].

The spin Hall angle—defined as  $\theta_{\text{SH}} = I_M^{S_z}/I_1$ —is shown in Fig. 4(b), where we confirm large values obtained from the Kubo formula as well as the detrimental effect of clustering of Au adatoms. While both Kubo and LB formula calculations predict  $\theta_{\text{SH}} \approx 0.1$  close to the CNP, thermal broadening effects included in LB formula calculations can reduce  $\theta_{\text{SH}}$  by up to one order of magnitude [see Fig. 4(b)]. By comparing Fig. 4(b) with Fig. S4 of Supplemental Material [30], we find that the hypothetical case of homogeneous Rashba SOC, due to Au adatoms covering every hexagon in Fig. 1, generates the SHE akin to the intrinsic one in finite-size two-dimensional electron gases [43,44]. Its  $\theta_{\text{SH}}$  exhibits a wider peak (centered at  $E_F = 0.3\gamma_0$  due to doping of graphene by Au adatoms) of smaller magnitude than in the case of randomly scattered Au adatoms. Thus, adatom-induced resonant scattering [13] plays an important role in generating a large extrinsic SHE.

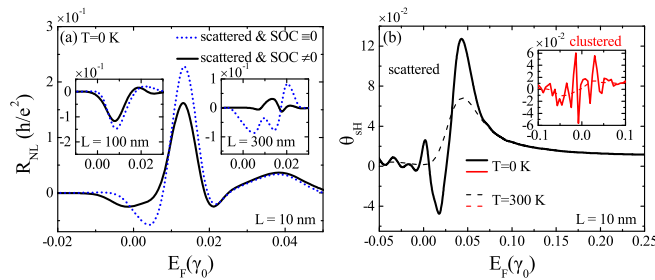


FIG. 4. (a) Nonlocal resistances for six-terminal graphene in Fig. 1 with  $n_i = 15\%$  of scattered Au adatoms, fixed channel width  $W = 50$  nm, and several channel lengths:  $L = 10$  nm (main frame);  $L = 100$  nm (left inset); and  $L = 300$  nm (right inset). Dotted lines plot  $R_{\text{NL}}$  when all SOC terms in Eq. (1) are switched off ( $\text{SOC} \equiv 0 \Leftrightarrow V_I = V_R = 0$ ). (b) Spin Hall angle, obtained from LB formula calculations, for the same concentration of Au adatoms which are scattered (main frame) or clustered (inset). All curves are averaged over ten disorder configurations.

Figure 4(a) shows  $R_{\text{NL}}$  as a function of energy and for various channel lengths  $L$ . Most notably, we find a nonzero  $R_{\text{NL}}$  even when all SOC terms are switched off ( $V_R = V_I = 0$ ) in Eq. (1) while keeping random on-site potential  $\mu \neq 0$  due to Au adatoms unchanged. Furthermore, we find a complex sign change of  $R_{\text{NL}}$  in Fig. 4(a) with increasing channel length from  $L = 10$  nm to  $L = 300$  nm, which suggests the following interpretation. The total  $R_{\text{NL}}$  can have four contributions  $R_{\text{NL}} = R_{\text{NL}}^{\text{SHE}} + R_{\text{NL}}^{\text{Ohm}} + R_{\text{NL}}^{\text{qb}} + R_{\text{NL}}^{\text{pd}}$ , assuming they are additive after disorder averaging. For an unpolarized charge current injected from lead 1 (i.e., electrons injected from lead 2):  $R_{\text{NL}}^{\text{SHE}}$  generated by the combined direct and inverse SHE has a positive sign; trivial Ohmic contribution  $R_{\text{NL}}^{\text{Ohm}}$  due to classical diffusive charge transport [16,18] has a positive sign;  $R_{\text{NL}}^{\text{qb}}$  is the negative quasiballistic contribution arising due to direct transmission  $T_{32} \neq 0$  from lead 2 to lead 3 (see Fig. S6 in Supplemental Material [30]), as observed previously in SHE experiments on multiterminal gold devices [28]; finally,  $R_{\text{NL}}^{\text{pd}}$  is a positive contribution specific to Dirac materials where evanescent wave functions generate pseudodiffusive transport [45] close to the CNP characterized by two-terminal conductance scaling as  $G \propto 1/L$  even in perfectly clean samples as long as their geometry satisfies  $W > L$  (see Fig. S5 in Supplemental Material [30]).

Thus, in a device with  $W > L$ , such as  $W = 50$  nm and  $L = 10$  nm in the main frame of Fig. 4(a), the positive sign  $R_{\text{NL}}$  is dominated by  $R_{\text{NL}}^{\text{pd}}$ , which can be larger than in the case of perfectly clean graphene in Fig. S5 of Supplemental Material [30] due to scattering from impurities (of uniform strength) at the CNP [46]. The negative sign of  $R_{\text{NL}}$  in the two insets in Fig. 4(a) in the absence of SOC and for  $L > W$  suggests that  $R_{\text{NL}}^{\text{Ohm}}$  can be safely neglected in our samples due to small  $n_i$ —we estimate the mean free path  $\ell = 300-400$  nm for  $n_i = 15\%$ , so that when diffusive transport regime sets in for  $\ell < L$ , the Ohmic contribution  $R_{\text{NL}}^{\text{Ohm}} \propto \exp(-\pi L/W)$  [16,18] is already negligible due to  $L/W \gg 1$ . Therefore, for  $L > W$  the main competition is between  $R_{\text{NL}}^{\text{qb}}$  with a negative sign and  $R_{\text{NL}}^{\text{SHE}}$  with a positive sign, as found in the two insets in Fig. 4(a). The existence of background contributions to  $R_{\text{NL}}$  that do not originate from the SHE, and can be even larger than  $R_{\text{NL}}^{\text{SHE}}$ , could explain the insensitivity of the total  $R_{\text{NL}}$  to the applied external in-plane magnetic field observed in some experiments [15,16].

The difficulty in clarifying the dominant contribution to  $R_{\text{NL}}$  could be resolved by detecting its sign change as a function of the channel length  $L$  in Fig. 1. An alternative is to design a setup where  $R_{\text{NL}}^{\text{Ohm}}$ ,  $R_{\text{NL}}^{\text{qb}}$ , and  $R_{\text{NL}}^{\text{pd}}$  are negligible so that  $R_{\text{NL}}^{\text{SHE}}$  can be isolated. We propose such a setup in Fig. S7 of Supplemental Material [30], where adatoms are removed in the channel. When such a channel is sufficiently long,  $R_{\text{NL}}^{\text{pd}} = 0$  due to  $L > W$  and  $R_{\text{NL}}^{\text{Ohm}}, R_{\text{NL}}^{\text{qb}} \rightarrow 0$  due to the absence of impurity scattering in the channel, so that

mediative spin current  $I_M^S$  generated by the direct SHE in the first crossbar arrives conserved [44] at the second crossbar where it is converted into  $V_{NL}$  by the inverse SHE. Indeed, Fig. S8 of Supplemental Material [30] demonstrates that  $R_{NL}$  and  $\theta_{SH}$  in this setup are unambiguously related, since they both display a sharp peak at virtually the same  $E_F$  very close to the CNP.

A. W. Cummings and J. H. Garcia are acknowledged for critical reading of the manuscript. This project has received funding from the European Union's Horizon 2020 research and innovation programme under grant agreement No. 696656. S.R. acknowledges Funding from the Spanish Ministry of Economy and Competitiveness and the European Regional Development Fund (Project No. FIS2015-67767-P (MINECO/FEDER)), the Secretaria de Universidades e Investigación del Departamento de Economía y Conocimiento de la Generalidad de Cataluña, and the Severo Ochoa Program (MINECO, Grant No. SEV-2013-0295). We acknowledge computational resources from PRACE and the Barcelona Supercomputing Center (Mare Nostrum), under Project No. 2015133194. J. M. M.-T. was supported as a Fulbright Colombia Scholar and by Colciencias (Departamento Administrativo de Ciencia, Tecnología e Innovación) of Colombia. B. K. N. was supported by United States National Science Foundation (NSF) Grant No. ECCS 1509094 and is grateful for the hospitality of Centre de Physique Théorique de Grenoble-Alpes where part of this work was done. S. O. V. acknowledges support from the European Research Council under Grant Agreement No. 308023 SPINBOUND. The supercomputing time was provided by Extreme Science and Engineering Discovery Environment (XSEDE), which is supported by NSF Grant No. ACI-1053575.

\*bnikolic@udel.edu

†stephan.roche@icn2.cat

- [1] G. Vignale, *J. Supercond. Novel Magn.* **23**, 3 (2010).
- [2] J. Sinova, S. O. Valenzuela, J. Wunderlich, C. H. Back, and T. Jungwirth, *Rev. Mod. Phys.* **87**, 1213 (2015).
- [3] Y. Kato, R. C. Myers, A. C. Gossard, and D. D. Awschalom, *Science* **306**, 1910 (2004); J. Wunderlich, B. Kaestner, J. Sinova, and T. Jungwirth, *Phys. Rev. Lett.* **94**, 047204 (2005); S. O. Valenzuela and M. Tinkham, *Nature (London)* **442**, 176 (2006); E. Saitoh, M. Ueda, H. Miyajima, and G. Tatara, *Appl. Phys. Lett.* **88**, 182509 (2006).
- [4] A. H. Castro Neto, F. Guinea, N. M. R. Peres, K. S. Novoselov, and A. K. Geim, *Rev. Mod. Phys.* **81**, 109 (2009); A. Ferrari *et al.*, *Nanoscale* **7**, 4598 (2015).
- [5] S. Roche *et al.*, *2D Mater.* **2**, 030202 (2015). W. Han, R. K. Kawakami, M. Gmitra, and J. Fabian, *Nat. Nanotechnol.* **9**, 794 (2014);
- [6] D. Huertas-Hernando, F. Guinea, and A. Brataas, *Phys. Rev. B* **74**, 155426 (2006); M. Gmitra, S. Konschuh, C. Ertler, C. Ambrosch-Draxl, and J. Fabian, *Phys. Rev. B* **80**, 235431 (2009); A. H. Castro Neto and F. Guinea, *Phys. Rev. Lett.* **103**, 026804 (2009); V. K. Dugaev, E. Ya. Sherman, and J. Barnas, *Phys. Rev. B* **83**, 085306 (2011).
- [7] N. Tombros, C. Jozsa, M. Popinciuc, H. T. Jonkman, and B. J. Van Wees, *Nature (London)* **448**, 571 (2007).
- [8] K. Pi, W. Han, K. M. McCreary, A. G. Swartz, Y. Li, and R. K. Kawakami, *Phys. Rev. Lett.* **104**, 187201 (2010).
- [9] B. Dlubak *et al.*, *Nat. Phys.* **8**, 557 (2012).
- [10] M. H. D. Guimarães, P. J. Zomer, J. Ingla-Aynes, J. C. Brant, N. Tombros, and B. J. van Wees, *Phys. Rev. Lett.* **113**, 086602 (2014); M. Drögeler, F. Volmer, M. Wolter, B. Terres, K. Watanabe, T. Taniguchi, G. Güntherodt, C. Stampfer, and B. Beschoten, *Nano Lett.* **14**, 6050 (2014); M. Venkata Kamalakar, C. Groenvelde, A. Dankert, and S. P. Dash, *Nat. Commun.* **6**, 6766 (2015); B. Raes, J. E. Scheerder, M. V. Costache, F. Bonell, J. F. Sierra, J. Cuppens, J. Van de Vondel, and S. O. Valenzuela, *Nat. Commun.* **7**, 11444 (2016).
- [11] J. Balakrishnan *et al.*, *Nat. Commun.* **5**, 4748 (2014).
- [12] J. Balakrishnan, G. K. Wai Koon, M. Jaiswal, A. H. Castro Neto, and B. Özyilmaz, *Nat. Phys.* **9**, 284 (2013).
- [13] A. Ferreira, T. G. Rappoport, M. A. Cazalilla, and A. H. Castro Neto, *Phys. Rev. Lett.* **112**, 066601 (2014).
- [14] H.-Y. Yang, C. Huang, H. Ochoa, and M. A. Cazalilla, *Phys. Rev. B* **93**, 085418 (2016).
- [15] Y. Wang, X. Cai, J. Reutt-Robey, and M. S. Fuhrer, *Phys. Rev. B* **92**, 161411 (2015).
- [16] A. A. Kaverzin and B. J. van Wees, *Phys. Rev. B* **91**, 165412 (2015).
- [17] R. V. Gorbachev *et al.*, *Science* **346**, 448 (2014).
- [18] D. A. Abanin, A. V. Shytov, L. S. Levitov, and B. I. Halperin, *Phys. Rev. B* **79**, 035304 (2009).
- [19] D. V. Tuan, F. Ortmann, D. Soriano, S. O. Valenzuela, and S. Roche, *Nat. Phys.* **10**, 857 (2014); D. V. Tuan, F. Ortmann, A. W. Cummings, D. Soriano, and S. Roche, *Sci. Rep.* **6**, 21046 (2016); D. Van Tuan and S. Roche, *Phys. Rev. Lett.* **116**, 106601 (2016).
- [20] C.-L. Chen, C.-R. Chang, and B. K. Nikolić, *Phys. Rev. B* **85**, 155414 (2012).
- [21] P. Štředa, *J. Phys. C* **15**, L717 (1982).
- [22] N. A. Sinitsyn, J. E. Hill, H. Min, J. Sinova, and A. H. MacDonald, *Phys. Rev. Lett.* **97**, 106804 (2006).
- [23] I. A. Ado, I. A. Dmitriev, P. M. Ostrovsky, and M. Titov, *Phys. Rev. Lett.* **117**, 046601 (2016); M. Milletari and A. Ferreira, *Phys. Rev. B* **94**, 134202 (2016).
- [24] E. Sutter, P. Albrecht, B. Wang, M.-L. Bocquet, L. Wu, Y. Zhu, and P. Sutter, *Surf. Sci.* **605**, 1676 (2011).
- [25] K. Pi, K. M. McCreary, W. Bao, W. Han, Y. F. Chiang, Y. Li, S.-W. Tsai, C. N. Lau, and R. K. Kawakami, *Phys. Rev. B* **80**, 075406 (2009); M. I. Katsnelson, F. Guinea, and A. K. Geim, *Phys. Rev. B* **79**, 195426 (2009); K. M. McCreary, K. Pi, A. G. Swartz, W. Han, W. Bao, C. N. Lau, F. Guinea, M. I. Katsnelson, and R. K. Kawakami, *Phys. Rev. B* **81**, 115453 (2010).
- [26] A. Cresti, D. Van Tuan, D. Soriano, A. W. Cummings, and S. Roche, *Phys. Rev. Lett.* **113**, 246603 (2014).
- [27] M. Büttiker, *Phys. Rev. Lett.* **57**, 1761 (1986).
- [28] G. Mihajlović, J. E. Pearson, M. A. Garcia, S. D. Bader, and A. Hoffmann, *Phys. Rev. Lett.* **103**, 166601 (2009).
- [29] Z. Wang, H. Liu, H. Jiang, and X. C. Xie, *Phys. Rev. B* **94**, 035409 (2016).

- [30] See Supplemental Material (which includes Refs. [31–33]) at <http://link.aps.org/supplemental/10.1103/PhysRevLett.117.176602> for details on the validation tests of our real-space Kubo formula for  $\sigma_{\text{SH}}$ ; comparison of  $\theta_{\text{SH}}$  for Au vs Tl adatoms; and LB formula calculations of  $R_{\text{NL}}$  and  $\theta_{\text{SH}}$  on additional clean and disordered multiterminal graphene geometries.
- [31] C. L. Kane and E. J. Mele, *Phys. Rev. Lett.* **95**, 226801 (2005).
- [32] L. Sheng, D. N. Sheng, C. S. Ting, and F. D. M. Haldane, *Phys. Rev. Lett.* **95**, 136602 (2005).
- [33] K. Kazymyrenko and X. Waintal, *Phys. Rev. B* **77**, 115119 (2008); M. Wimmer and K. Richter, *J. Comput. Phys.* **228**, 8548 (2009).
- [34] C. Weeks, J. Hu, J. Alicea, M. Franz, and R. Wu, *Phys. Rev. X* **1**, 021001 (2011).
- [35] A. Avsar, J. H. Lee, G. K. Wai Koon, and B. Özyilmaz, *2D Mater.* **2**, 044009 (2015).
- [36] A. Weisse, G. Wellein, A. Alvermann, and H. Fehske, *Rev. Mod. Phys.* **78**, 275 (2006).
- [37] S. Roche and D. Mayou, *Phys. Rev. Lett.* **79**, 2518 (1997); S. Roche, *Phys. Rev. B* **59**, 2284 (1999); A. Ferreira and E. R. Mucciolo, *Phys. Rev. Lett.* **115**, 106601 (2015).
- [38] F. Ortmann and S. Roche, *Phys. Rev. Lett.* **110**, 086602 (2013); F. Ortmann, N. Leconte, and S. Roche, *Phys. Rev. B* **91**, 165117 (2015).
- [39] J. H. Garcia, L. Covaci, and T. G. Rappoport, *Phys. Rev. Lett.* **114**, 116602 (2015).
- [40] T. L. van den Berg, L. Raymond, and A. Verga, *Phys. Rev. B* **84**, 245210 (2011); J. H. Garcia and T. G. Rappoport, *2D Mater.* **3**, 024007 (2016).
- [41] A. Dyrdal, V. K. Dugaev, and J. Barnas, *Phys. Rev. B* **80**, 155444 (2009).
- [42] C. W. Groth, M. Wimmer, A. R. Akhmerov, and X. Waintal, *New J. Phys.* **16**, 063065 (2014).
- [43] B. K. Nikolić, L. P. Zárbo, and S. Souma, *Phys. Rev. B* **72**, 075361 (2005); L. Sheng, D. N. Sheng, and C. S. Ting, *Phys. Rev. Lett.* **94**, 016602 (2005); B. K. Nikolić and R. L. Dragomirova, *Semicond. Sci. Technol.* **24**, 064006 (2009).
- [44] B. K. Nikolić, L. P. Zárbo, and S. Souma, *Phys. Rev. B* **73**, 075303 (2006).
- [45] J. Tworzydło, B. Trauzettel, M. Titov, A. Rycerz, and C. W. J. Beenakker, *Phys. Rev. Lett.* **96**, 246802 (2006); P.-H. Chang, F. Mahfouzi, N. Nagaosa, and B. K. Nikolić, *Phys. Rev. B* **89**, 195418 (2014).
- [46] M. Titov, *Europhys. Lett.* **79**, 17004 (2007).